Accepted manuscript (author version)

To appear in:

Iranian Journal of Earth Sciences (Iran J. Earth. Sci.)

E-ISSN: 2228-785X **Print ISSN:** 2008-8779

This PDF file is not the final version of the record. This version will undergo further copyediting, typesetting, and production review before being published in its definitive form. We are sharing this version to provide early access to the article. Please be aware that errors that could impact the content may be identified during the production process, and all legal disclaimers applicable to the journal remain valid.

Received: 12 August 2025

Revised: 1 October 2025

Accepted: 12 November 2025

Accepted manuscript

CC BY 4.0 https://creativecommons.org/licenses/by/4.0/

Accepted manuscript (author version)

DOI: 10.57647/ijes.2026.18033

Original Research

Thermobarometric studies of the Upper Triassic basic volcanic rocks of Pol-e Sefid (Central Alborz-Iran): Extensional regime and petrogenesis

Saeid Samarbakhsh[1], Mohammad Hashem Emami[1]*, Seyed Mojtaba Mortazavi[2], Mansour Vosoughi Abedini[1], Abdollah Yazdi[3]*

[1] Department of Earth Sciences, SR.C., Islamic Azad University, Tehran, Iran

[2] Department of Mining Engineering, Sava.C., Islamic Azad University, Savadkooh, Iran

[3] Department of Geology, Kah.C., Islamic Azad University, Kahnooj, Iran

* Corresponding authors: hashememami@yahoo.com , abdollah.yazdi@iau.ac.ir

© The Author(s), 2025

Abstract

A new study of the volcanic rocks of the Upper Triassic of Central Albarz, northern Iran, has been conducted. This area is about 200 km from Tehran, near Pol-e-Sefid (Khatirkouh). Researchers chose this location due to the lack of detailed studies on these rocks and the area's tectonic regime. One reason for this gap is the severe alteration of the volcanic rocks. Given its central location, this research can greatly enhance our understanding of the techno-magmatic environment, especially in central Alborz. Thus, field studies, petrography, and thermobarometry were done on these rocks. The most common formations in the region, ranging in age from Lower Carboniferous to Middle Jurassic, include the Mobarak, Dorood, Ruteh, Elika, and Shemshak formation. The primary minerals in the region's volcanic rocks (which include basalt, andesite, trachyandesite, and dolerite) are clinopyroxene, olivine, and plagioclase. These volcanic rocks exhibit textures ranging from porphyritic to mega-porphyritic, with matrices that are microlitic, glomeroporphyritic. Chemical analyses of the minerals reveal that the clinopyroxenes are predominantly diopside and augite. Additionally, the plagioclases are classified as oligoclase, labradorite, and bytownite. Based on thermobarometric diagrams and calculations, the formation temperatures are determined to be between 850 and 1100 °C, and pressures range from 6.10 to 8.5 kbar. Finally, the investigation of the tectonic setting of these rock masses based on the chemistry

CC BY 4.0 https://creativecommons.org/licenses/by/4.0/

of clinopyroxene and plagioclase minerals indicates the formation of the region's rocks in an extensional environment.

Keywords: Basalt, Thermobarometry, Upper Triassic, Pol-e Sefid, Iran

1. Introduction

The Iran was located along the northeastern margin of Gondwana during the Permian. In the Early Triassic, it moved northward past the equator, eventually encountering the southern margin of the Laurasia continent in the Late Triassic. The temporal and location of volcanic stones in the Alborz area has a significant control over their geochemical diversity. The temperature and pressure of the Alborz Zone volcanic rocks were performed using thermobarometry studies by various researchers. The point analysis of minerals—especially phenocrysts—for determining their chemical composition, classification, and nomenclature is of great significance. Such analyses enable the calculation of crystallization temperatures and pressures, final mineral equilibria, magma ascent rates, and the depth of emplacement of igneous bodies. Furthermore, the chemical composition of minerals reflects the physicochemical conditions of the magma, including temperature, pressure, and oxygen fugacity. As a result, minerals serve as valuable tools for assessing the physicochemical environment of both the magma and the surrounding rock-forming system. Minerals such as biotite, pyroxene, amphibole, and feldspar are particularly useful in microprobe studies (Larson et al., 1938; Finch and Anderson, 1930; Fenner, 1926).

Future advances in in-situ analysis, thermodynamic modeling, and integration with geophysical data will further expand the utility of thermobarometry in tectonic research (Sayari, 2011; Goncalves et al., 2013; Sayari and Sharifi, 2014; Dabiri et al., 2018; Mollai et al., 2021; Arjmandzadeh et al., 2021; Talebian Borojenie et al., 2025).

Studies from tectonically active regions such as the Central Alborz in Iran, the Basin and Range Province in the United States, and the Andes in South America demonstrate the critical role of thermobarometry in supporting tectonic interpretations. In the Central Alborz, for example, thermobarometric analyses of pyroxene and plagioclase minerals from Mesozoic volcanic rocks reveal evidence of magma ascent through an extensional crustal regime. This setting is closely linked to the subduction of the Neotethys Ocean and the development of a back-arc extensional

Accepted manuscript (author version)

CC BY 4.0 https://creativecommons.org/licenses/by/4.0/

environment, which facilitated the formation of shallow magmatic reservoirs and promoted rapid magma emplacement (Doroozi et al., 2017; Rostami et al., 2018; Shahabi et al., 2021).

Iran experienced three major phases of magmatic expansion throughout the Paleozoic. The Early Triassic phase marks a critical stage of tectonic rupture, coinciding with the opening of the Neotethyan oceanic basin (Ghasemi and Jamshidi, 2012, 2013). This phase is characterized by basaltic volcanism in the Alborz and other parts of Iran, such as the Sanandaj–Sirjan zone (Berberian and King, 1981). In the Central Alborz, the primary Triassic carbonates are overlain by shales and sandstones of Late Triassic age. During this time, an extensional tectonic phase associated with alkaline magmatic activity eruption (Berberian and King, 1981; Berberian and Berberian, 1981). The presence of alkaline extrusive rocks and volcanic-sedimentary sequences interbedded with the Late Triassic shales and sandstones indicates the existence of an extensional regime in the Central Alborz (Nazari et al., 2004; Ghasempour et al., 2014). The evolution of this regime likely contributed to the formation of the Caspian and Black Sea basins during the Late Middle Jurassic (Nazari, 2004). In the Late Triassic, the structural characteristics of the lower part of the Shemshak Formation reveal a significant extensional system, as evidenced by the presence of multiple normal faults. Variations in the thickness of this part of the formation are attributed to the activity of major normal or detachment faults in the Central Alborz (Nazari and Shahidi, 2011). Concurrently, with the closure of the Paleotethys, the subduction of the Neotethys commenced in the Zagros region, generating an extensional setting in the back-arc area. This tectonic environment led to deep faulting and the eruption of alkaline basaltic magmas—such as the basalts of Jaban, Semnan, Toi (Damghan), and Jajarm in the Central Alborz and other parts of Iran—which occurred simultaneously with the deposition of the Shemshak Formation. During the Upper Triassic, the Central Alborz and Central Iran were situated in tropical latitudes near the equator, creating optimal conditions for bauxitization due to intense weathering of basalts and other materials. Several factors contributed to the formation of bauxite deposits: equatorial hot and humid climate; availability of parent material (basalts); presence of suitable host rocks (fractures and karst systems in carbonate units such as the Elika and Shotori formations); and the synchronous deposition of the Shemshak Formation, which protected the bauxites from erosion. Geological evidence and the close spatial association of most bauxite deposits with the shales of the Shemshak Formation suggest that clay-rich materials also played a role in the bauxitization process. Under the influence

Accepted manuscript (author version)

CC BY 4.0 https://creativecommons.org/licenses/by/4.0/

Accepted manuscript (author version)

of alkaline magmatic activity, basalts were initially altered to clay, with immobile elements such as aluminum and iron remaining behind to form residual bauxite. Where clays were already present in the shales or limestones, they could more readily participate in bauxitization, facilitating the accumulation of aluminum-rich lateritic profiles.

The aim of this research is to study and investigate the chemistry of pyroxene and plagioclase minerals in volcanic rocks of the Pol Sefid region, so that by using the results of chemical analysis, drawing related diagrams, and numerical calculations, the tectonomagmatic environment of their formation, the type of magma, and petrological processes can be understood.

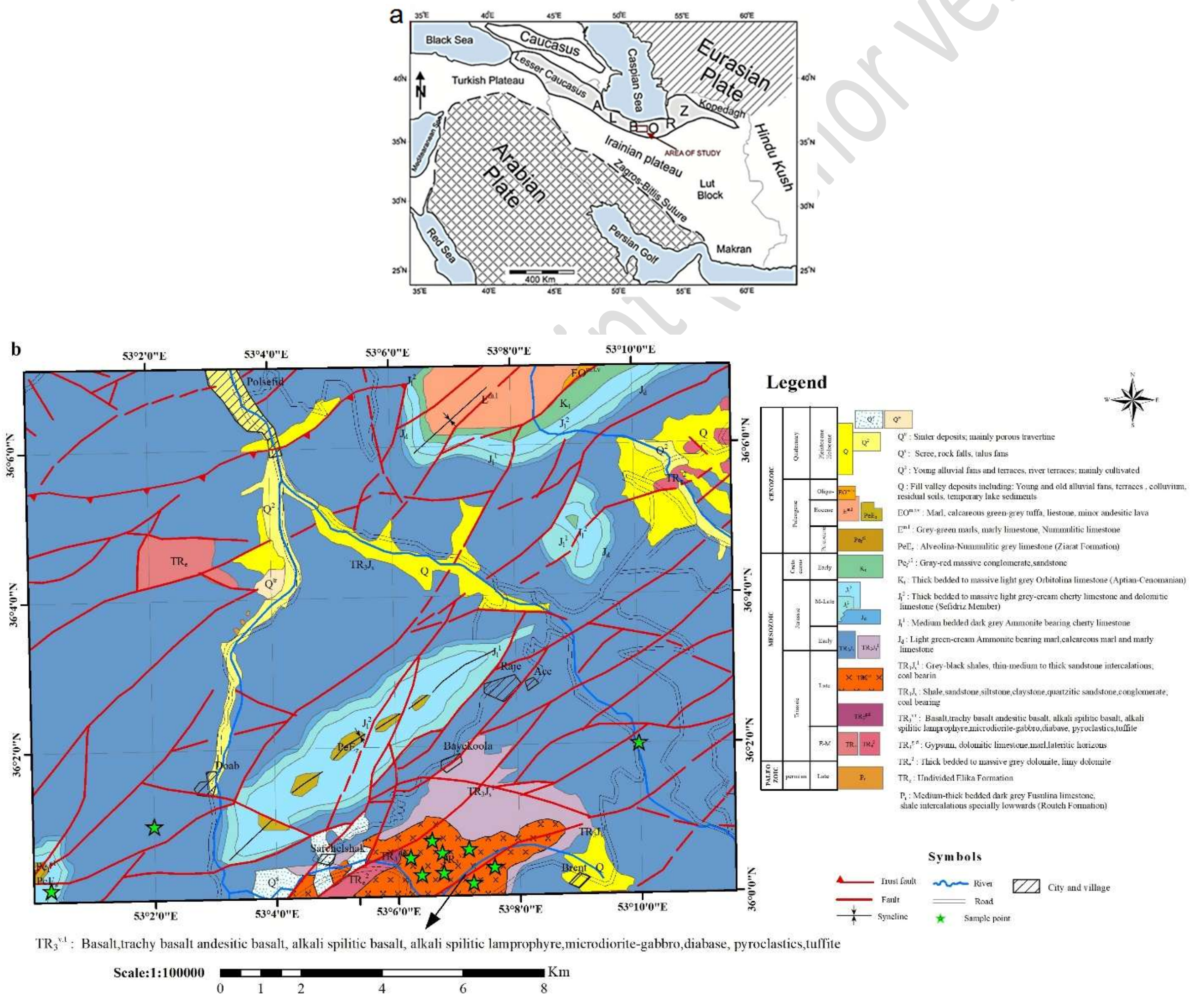

Figure 1. a- General tectonic map of Iran with Arabian and Eurasian plate and the location of studied area in Central Alborz zone (Doroozi et al., 2018). b- Geological map simplified from the 1:100,000 map of Ghaem Shahr, Kiasar(Saeedi and Akbarpour, 1992), Pol Sefid and the map of Semnan with a scale of 1:250,000 (Samadian et al., 1994). Note the star sign inside the figure.

CC BY 4.0 https://creativecommons.org/licenses/by/4.0/

2. Geology of the Region

The study area is part of the Alborz Mountains and belongs to the Central Alborz zone(Fig. 1a). Geographically, it is located between longitudes 53′00″ to 53′10″ E and latitudes 36′00″ to 36′09″ N (Fig. 1b). The lithostratigraphic units present in the area range in age from the Triassic to the Quaternary. The Elika Formation (Triassic) in the Alborz consists of middle and upper carbonate sections and is composed mainly of limestone and dolomite(Vahabzadeh, 2007). Based on field studies, the lower vermiculated limestones in the Pol-e Sefid quarry and its surroundings are absent, with only the second (dolomitic limestone) and the upper members (the Varsek member) are presented. An important feature of the Elika Formation in the area is the development of karst. The Shemshak Formation, comprising sandstone, siltstone, and shale that occur alternately and includes a coal seam in its main section. In addition to the Jurassic Shemshak Formation, the Lar Formation is also present in the region, characterized by nodules and boudins with white or purplish shades(Assereto, 1966a). In the Central Alborz, Upper Triassic volcanic rocks are typically represented by basaltic–splintered pyroclastics that overlie the Karsted surfaces of the Elika Formation (Middle Triassic) or older units. From the outskirts of Damavand to Firozkuh and northern Semnan, these pyroclastic rocks are identified by a key dark layer that overlies the light-colored Triassic carbonates (Elika Formation). In many cases, after emplacement, due to re-equilibration processes, these pyroclastic rocks have been transformed into ferruginous horizons or bauxite lenses; in some localities, such as in Sangasar (Semnan), Toi–Darvar (Bakhteh, Damghan), and Sangarud (Lushan), they have even been used as refractory materials. Around the Pol-e Sefid area, Upper Triassic volcanic rocks, which are gray to black, exhibit intense weathering and a gentler dip compared to the Elika Formation (Fig. 1b). The Tizkuh (Upper Karstic) unit, belonging to the overlying sequence, is composed of conglomerate, sandstone, and yellowish arenaceous limestone at the base, with the overlying carbonate limestones forming a sedimentary sequence(Khosrow Tehrani, 2007). In the region, conglomerates and sandstones predominate, and in some areas, volcanic rocks are intercalated; gradually, these transition into shallow-marine, nummulitic limestones of the lower Eocene. In the Middle Eocene, a significant thickness—about 3000 meters—of tufaceous and green tufite deposits in the south of the collapsing Alborz basin is observed, eventually passing into shallow and evaporitic Upper Eocene sediments. At the Eocene–Oligocene boundary, the Pyrenean orogeny caused widespread exhumation of the Southern

Accepted manuscript (author version)

CC BY 4.0 https://creativecommons.org/licenses/by/4.0/

Accepted manuscript (author version)

Alborz, resuting the absence of Oligocene sequences. However, in the intermontane basins of these highlands, sequences of oxidized clay sediments occur, whose lithological characteristics are similar to those of the Neogene (Upper Red Formation of Central Iran). Lithologically, the Karaj Formation is mainly composed of tuff, shale, tuffaceous shale, tuff sandstone, and conglomerate. Old alluvial fans and terraces are the youngest deposits(Quaternary) in the studied. The locations of the sampled points are listed in Table 1.

3. Methodology

During fieldwork, a systematic sampling campaign was conducted, resulting in the collection of 100 rock samples. From these, 50 thin sections were prepared and examined under a polarizing microscope. For thermobarometric analysis of the regional rocks, 10 representative thin sections were selected based on petrographic and mineralogical characteristics. A total of 15 point analyses were conducted on pyroxene and plagioclase minerals using an electron microprobe (EPMA) at the International Consortium in Binalod in Tehran(Iran). The analyses were performed with a HORIBA XGT-7200 instrument, operating at an accelerating voltage of 50 kV and a beam current of 1 μA. The measurement accuracy of this device was high, and the data may have an error of about (±1-2%Wt). Each measurement was carried out on a spot with a diameter of 10 microns, with a counting time of 80 seconds per point. Structural formulas for the analyzed minerals were calculated using customized Excel spreadsheets designed for mineral chemistry computations (Tables 2 and 3)**.**

4. Petrography

Out of the 40 collected samples, 40 were selected based on their uniqueness and durability, and corresponding thin sections were prepared. After the thin section studies, all the rocks were divided into three groups: extrusive igneous, intrusive igneous, and sedimentary. Below, we examine the rocks of the area.

- **Basalt:**

The basalt exhibits a hyaloclastic texture, porphyritic with a microlitic groundmass and vesicular to glassy appearance; plagioclase occurs in various shapes and sizes euhedral and anhedral forms within the rock. Based on optical properties and refractive indices, the plagioclase in these rocks seems ranges from labradorite to anorthite. Pyroxene appears in a well-formed to subhedral shape

CC BY 4.0 https://creativecommons.org/licenses/by/4.0/

and in some cases as twin crystals. These pyroxenes, based on their optical characteristics, are probably of the augite type. Olivine occurs in both euhedral and anhedral forms in the samples; these olivines have been completely altered to chlorite, opaque minerals, saponite, and iddingsite. The groundmass is composed of microlitic plagioclase, pyroxene, opaque minerals, and glass. In many instances, the glass in the groundmass has transformed due to devitrification into stringy or radial chlorite(Fig. 2a, b).

- **Trachybasalt:**

This rock shows a porphyritic texture with a microlitic groundmass. The pyroxenes are subhedral to anhedral and are identified as augite; they are typically observed as isolated crystals and are sparsely distributed within the groundmass. It is notable that these pyroxenes are often replaced by calcite and opaque minerals. Olivine is present in both euhedral and anhedral forms, and in some cases, it has been completely replaced by opaque minerals and iddingsite. The groundmass is comprised of microlitic plagioclase, alkali feldspar, pyroxene, olivine, and opaque minerals. In these samples, many mafic minerals present in the groundmass have been replaced by opaque minerals. The groundmass texture, resulting from the flowage of lava containing microlitic plagioclase and alkali feldspar showing trachytic texture. Amphiboles can be identified by their blade-like shapes and cross-cutting extinction in certain sections. Accessory minerals include opaque minerals with euhedral and anhedral crystals, scattered throughout the groundmass(Fig. 2f).

- **Olivine Basalt:**

This rock has a porphyritic texture with a microlitic groundmass, and pyroxene appears in euhedral shapes (sometimes as twin crystals) with greater abundance compared to olivine. Based on optical properties, these pyroxenes are seems to be augite. Olivine is presented in both euhedral to anhedral forms, and these minerals are often completely replaced by clinopyroxene, calcite, opaque minerals, and iddingsite. The groundmass is composed of microlitic plagioclase, fine-crystalline pyroxene, opaque minerals, and glass. In many cases, these minerals have altered into clay minerals, chlorite, and opaque minerals. Within the groundmass, quartz grains with reaction rims by fine pyroxene, altered plagioclase fragments with dissolution margins, and calcite grains are observed. In the groundmass, the interstitial spaces are filled by late-stage minerals such as quartz, calcite, chlorite, zeolite, and alkali feldspar (adularia). Plagioclase phenocrysts are occasionally completely replaced by chlorite and sericite minerals (Fig. 2c).

CC BY 4.0 https://creativecommons.org/licenses/by/4.0/

Accepted manuscript (author version)

- **Olivine Dolerite:**

This rock is characterized by a porphyritic texture with intergranular and intersertal groundmass, with plagioclase occurring in shapes ranging from euhedral to anhedral and exhibiting an albite-carlspad twins. The pyroxene occurs as isolated crystals and rarely as clusters within the groundmass. These pyroxenes, seems to be augite type. Olivine appears as euhedral to anhedral crystals with moderate abundance. These olivine crystals, are completely replaced by clinopyroxene, calcite, opaque minerals, and iddingsite is frequently observed. The groundmass is composed of microlitic plagioclase, pyroxene, fine-grained opaque minerals, and glass that has altered completely to chloritization. The open spaces within the groundmass are occupied by calcite and chlorite. Accessory minerals include isolated, euhedral to anhedral opaque minerals crystals dispersed throughout the rock. In some cases, these minerals are in forma of layers or bands (Fig. 2d, e).

Table 1. The sampling locations, phenocrysts mineral types in type rock Pole Sefid

Type rock	sampling locations	phenocrysts mineral types	texture
basalt	53° 6' 12.320" E 36° 0' 31.110" N 53° 6' 23.283" E 36° 0' 17.101" N 53° 6' 43.838" E 36° 0' 34.323" N 53° 6' 44.958" E 36° 0' 18.394" N 53° 7' 14.101" E 36° 0' 9.925" N 53° 9' 60.000" E 36° 1' 59.999" N	Plagioclases and pyroxene	Hyaloclastic and Porphyritic
Trachybasalt	53° 6' 33.805" E 36° 0' 44.54" N 53° 7' 10.195" E 36° 0' 37.20" N 53° 6' 33.731" E 36° 0' 44.745" N	Plagioclases and pyroxene	porphyritic
Olivine basalt	53° 0' 17.160" E 36° 0' 10.016" N 53° 1' 60.000" E 36° 0' 59.99" N 53° 7' 35.050" E 36° 0' 22.533" N	Plagioclases	microlitic porphyritic
Trachyandesite basalt	53° 7' 10.837" E 36° 0' 37.341" N 53° 7' 35.247" E 36° 0' 22.728" N 53° 2' 0.288" E 36° 1' 0.179" N	Plagioclases and pyroxene	microlitic porphyritic

CC BY 4.0 https://creativecommons.org/licenses/by/4.0/

Accepted manuscript (author version)

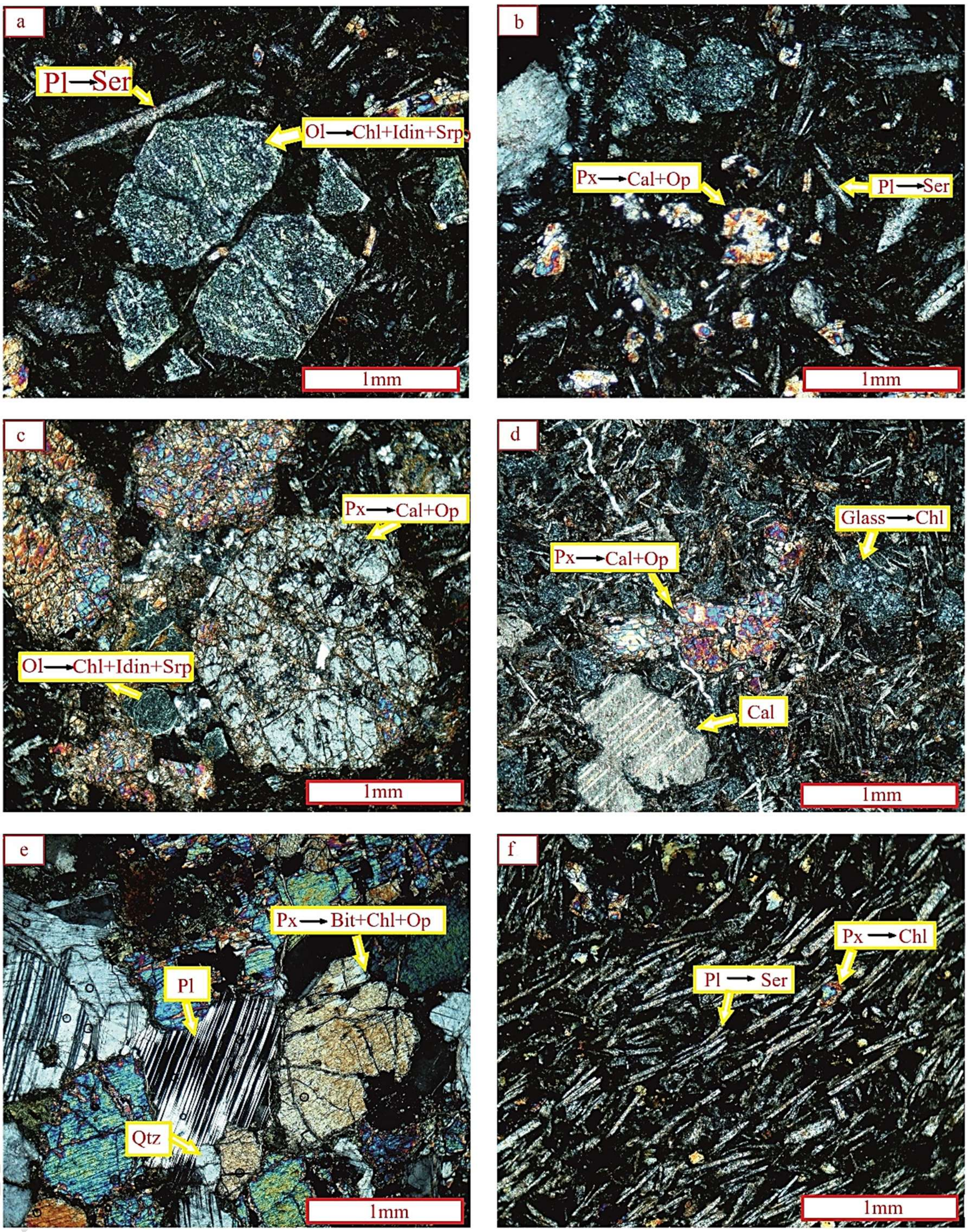

Figure 2. a- Plagioclase phenocryst in chloritized groundmass of basalt. b- Plagioclase and pyroxenes phenocryst in basalt. c- Olivine and pyroxenes phenocrysts in olivine basalt. d- A view of phenocrysts of pyroxene and chloritized glasses in dolerite. e- View of amorphous quartz, plagioclase, pyroxene in dolerite. f- A oriented feldspar microlites(trachytic texture) in trachybasalt.

CC BY 4.0 https://creativecommons.org/licenses/by/4.0/

Accepted manuscript (author version)

1. Mineral Chemistry:

The average chemical composition of the large clinopyroxene crystals in the basalts ranges from En21.24, Fs31.24, Wo47.76 to En30.67, Fs20.99, Wo55.81; in the olivine basalts from En50.80, Fs18.05, Wo30; and in the trachyandesitic basalts from En48.90, Fs18.64, Wo8.35 to En60.20, Fs21.05, Wo21.07 and in the trachybasalts from En45.57, Fs19.42, Wo34.35 to En52.63, Fs10.65, Wo42.70. As seen in Fig. 3, the pyroxenes in the studied samples are of the calcium–sodium type(Morimoto, 1988). Using an Excel spreadsheet for clinopyroxene calculations, the mineral types were determined and are presented below. Clinopyroxenes in alkaline rocks, compared to those in tholeiitic rocks, are enriched in TiO_2 and Na_2O and depleted in Cr_2O_3.

Table 2. Representative microprobe analysis of plagioclases in Pole Sefid, values are given in wt.%. The structural formula calculation is based on eight oxygens and cations are in apfu (atoms per formula unit).

Pl	A.38.1-1	A.38.1-2	A.38.1-3	A.38.2-1	A.38.2-2	A.38.2-3	B4-1	B4-2	B4-3	B-1	B-2	B-3
SiO_2	68.59	68.04	67.38	70.51	69.52	69.84	54.44	53.43	52.78	53.19	52.8	52.79
TiO_2	0.41	0.5	0.65	0.2	0.1	0.08	0.06	0.06	0.06	0.03	0.02	0.01
Al_2O_3	18.74	17.22	18.91	17.96	18.22	19.03	27.41	28.2	28.38	28.8	28.78	28.75
Fe_2O_3	1.37	3.18	3.07	0.81	0.42	0.58	0.69	0.74	0.72	0.59	0.44	0.62
CaO	1.37	1.42	1.39	2.29	1.79	1.66	12.09	13.07	13.57	14.39	14.68	14.56
Na_2O	8.81	8.4	7.88	7.57	9.29	8.32	4.5	3.77	3.62	2.42	2.33	1.96
K_2O	0.33	0.24	0.21	0.17	0.39	0.3	0.17	0.21	0.13	0.06	0.06	0.09
SO_3	0.15	0.3	0.13	0.32	0.07	0.08	0.14	0.14	0.14	0.12	0.12	0.12
MgO	0.09	0.57	0.25	0.05	0.12	0.02	0.14	0.13	0.18	0.15	0.12	0.06
Si	12.04	12.11	11.91	12.29	12.16	12.15	9.93	9.76	9.68	9.69	9.66	9.68
Ti	0.05	0.07	0.09	0.03	0.01	0.01	0.01	0.01	0.01	0.00	0.00	0.00
Al	3.88	3.61	3.94	3.69	3.76	3.90	5.89	6.07	6.13	6.18	6.21	6.21
Fe(ii)	0.20	0.47	0.45	0.12	0.06	0.08	0.11	0.11	0.11	0.09	0.07	0.10
Ca	0.26	0.27	0.26	0.43	0.34	0.31	2.36	2.56	2.67	2.81	2.88	2.86
Na	3.00	2.90	2.70	2.56	3.15	2.81	1.59	1.33	1.29	0.85	0.83	0.70
K	0.07	0.05	0.05	0.04	0.09	0.07	0.04	0.05	0.03	0.01	0.01	0.02
An	7.74	8.40	8.74	14.14	9.39	9.72	59.16	64.89	66.93	76.38	77.39	79.94
Ab	90.04	89.91	89.69	84.61	88.18	88.19	39.85	33.87	32.31	23.24	22.23	19.47
Or	2.22	1.69	1.57	1.25	2.44	2.09	0.99	1.24	0.76	0.38	0.38	0.59

CC BY 4.0 https://creativecommons.org/licenses/by/4.0/

Accepted manuscript (author version)

Table 3. Representative microprobe analysis of analcimes in Pole Sefid, values are given in wt.%. The structural formula calculation is based on six oxygens and cations are in apfu (atoms per formula unit).

px	Brant2-1	Brant2-2	Brant2-3	Brant2-4	2B-2-1	2B-2-2	2B-2-3	B.3-1	B.3-2	B.3-3	A10-1	A10-2	A10-3	A37-1	A37-2	A37-3	A38-1	A38-2	A38-3
SiO2	40.2	39.75	40.8	40.78	40.92	40.18	39.87	31.95	41.12	39.66	51.92	52.28	52.23	51.27	52.1	51.42	54.39	54.04	52.32
TiO2	1.74	2.19	2.23	2.14	1.78	2.49	2.74	2.19	2.11	2.52	0.37	0.38	0.32	0.27	0.21	0.58	0.12	0.15	0.38
Al2O3	5.17	4.99	4.56	5.82	4.73	5.47	5.29	6.23	6.28	5.84	0.78	1.18	0.66	1.1	0.82	2.54	1.35	1.46	2.54
Cr2O3	0.64	0.53	0.78	0.5	0.07	0.07	0.07	7.75	5	0.05	0.01	0.05	0.06	0.18	0.1	0.3	0.4	0.63	0.17
Fe2O3	13.02	12.15	10.07	13.12	14.61	14.73	15.63	15.56	11.35	15.18	20.21	14.91	20.06	13.75	13.25	8.36	5.4	4.12	6.69
MnO2	0.32	0.29	0.22	0.25	0.38	0.37	0.39	0.28	0.23	0.36	0.44	0.36	0.51	0.34	0.36	0.27	0.23	0.12	0.21
MgO	10.05	9.93	11.77	10.05	9.66	9.47	8.98	6.41	7.45	8.67	22.3	20.85	22.6	31.53	32.08	18.65	20.59	19.79	16.53
CaO	26.1	29.16	27.84	25.9	26.17	25.24	26.05	23.83	24.02	27.52	4.31	10.84	4.11	2.18	2.13	18.1	17.62	20.07	21.55
Na2O	1.82	0.01	0.87	0.35	1.39	1.64	0.63	3.05	0.53	0.01	0.09	0.12	0.08	0.06	0.02	0.18	0.21	0.24	0.31
K2O	0.08	0.08	0.03	0.19	0.02	0.06	0.01	0.1	0.2	0.02	0	0	0.01	0	0	0	0	0	0
Si	1.62	1.6	1.62	1.63	1.64	1.62	1.62	1.38	1.65	1.65	1.92	1.93	1.93	1.85	1.87	1.89	1.94	1.95	1.92
Al	0.25	0.24	0.21	0.27	0.22	0.26	0.25	0.32	0.3	0.28	0.07	0.03	0.05	0.05	0.03	0.11	0.06	0.05	0.08
Fe(iii)	0.75	0.59	0.64	0.51	0.69	0.69	0.59	1.06	0.25	0.54	0.12	0.12	0.12	0.35	0.32	0.12	0.02	0.05	0.08
Cr	0.02	0.02	0.02	0.02	0	0	0	0.26	0.16	0	0	0	0	0.01	0	0.01	0.01	0.02	0
Ti	0.05	0.07	0.07	0.06	0.05	0.08	0.08	0.07	0.06	0.08	0.02	0.01	0.01	0.01	0.01	0.02	0	0	0.01
Mn	0.01	0.01	0.01	0.01	0.01	0.01	0.01	0.01	0.01	0.01	0.01	0.01	0.01	0.01	0.01	0.01	0.01	0	0.01
Mg	0.6	0.6	0.7	0.6	0.58	0.57	0.54	0.41	0.45	0.52	1	1.24	1.15	1.7	1.71	1.02	1.11	1.06	0.9
Ca	1.13	1.26	1.19	1.11	1.13	1.09	1.13	1.1	1.03	1.19	0.64	0.17	0.43	0.08	0.08	0.71	0.68	0.78	0.85
Na	0.14	0	0.07	0.03	0.11	0.13	0.05	0.26	0.04	0	0.02	0.01	0.01	0	0	0.01	0.01	0.02	0.02
K	0	0	0	0.01	0	0	0	0.01	0.01	0	0	0	0	0	0	0	0	0	0

Plagioclase is the most abundant mineral in the region's rocks, occurring as both large crystals and microlites. In the Or–Ab–An ternary diagram (Fig. 3b), the plagioclase compositions of the regional igneous rocks plot in the field corresponding to labradorite and bytownite. The water vapor pressure, rapid ascent of magma, and the resulting disequilibrium conditions in the magma are factors that progressively decrease the anorthite content (Deer et al., 1991).

In Figure 4, the regional samples plot in the alkaline and shoshonitic fields in diagrams a and b, and, in terms of tectonic setting, they are located in the rift or extensional domain (Fig. 4 c and d).

This is observed in the chemical composition of the clinopyroxenes in the studied area. During partial melting, sodium and titanium tend to be incompatible and preferentially partition into the

Accepted manuscript (author version)

CC BY 4.0 https://creativecommons.org/licenses/by/4.0/

melt; therefore, lower TiO_2 concentrations in the melt indicate a depleted source, while higher values point to an enriched or less-depleted source—either a deep-seated (OIB) magma (Davis et al., 2011) or a subcontinental reprocessed magma(Mckenzie and Oniins, 1995). Oxygen fugacity plays a significant role in altering the liquidus temperature and the composition of both the melt and the crystallizing phases (France et al., 2010) and is a key factor controlling magmatic processes(Kilinc et al., 1983; Kress and Carmichael, 1991; Ottonello, 2001; Moretti, 2005; Botcharnikov, 2005). It also influences the crystallization sequence and the type of minerals formed. By using the diagram of $Al^{4+} + Na$ versus $Al^{6+} + 2Ti + Cr$—which is itself a function of the trivalent iron content in the pyroxenes—it is possible to estimate the oxygen fugacity. In such diagrams, samples that plot above the line defined by $Fe^{3+}=0$ indicate pyroxenes crystallized under high oxygen fugacity conditions, whereas those plotting below the line indicate low oxygen fugacity. Moreover, Cameron and Papike (1981) noted that the further a sample is from the Fe^{3+} line, the higher the oxygen fugacity in the formation environment. In the diagram for these samples, all points lie below the $Fe^{3+}=0$ line (Fig. 5).

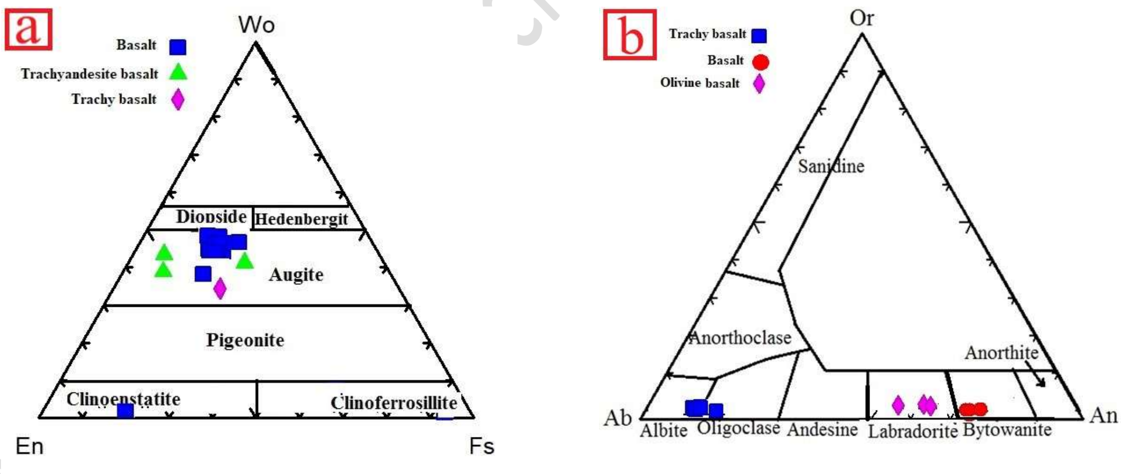

Figure 3. a-Naming of pyroxene of the studied sample based on the diagram (Deer et al., 1991). b- Determining the composition of igneous rock feldspar in the region (Deer et al., 1991).

CC BY 4.0 https://creativecommons.org/licenses/by/4.0/

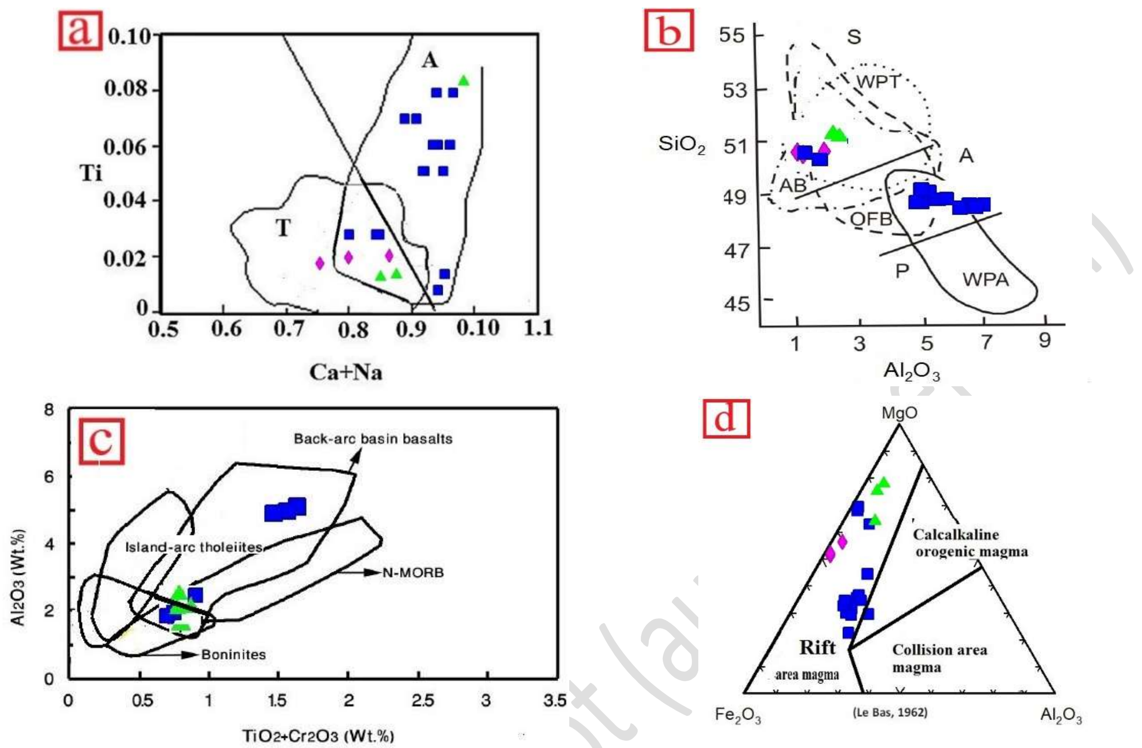

Figure 4. a- Diagram of Ti versus Ca + Na (T: tholeiitic basalts of island arcs and calc-alkaline, A: alkaline basalts) (Leterrier et al., 1982). b-Using clinopyroxene chemistry to determine magmatic series (Le Bas, 1962). c-Using clinopyroxene chemistry to deduce tectonic settings (Huot et al., 2002). d-Another clinopyroxene-based tectonic discrimination diagram (Leterrier et al., 1982).

Clinopyroxenes in alkaline rocks, when compared with those in tholeiitic rocks, show enrichment in TiO_2 and Na_2O and depletion in Cr_2O_3. During partial melting, sodium and titanium behave incompatibly; thus, lower TiO_2 concentrations in the melt suggest a depleted source and or continental contamination by mafic magma, whereas higher concentrations imply an enriched or less-depleted source—either a deep-seated (OIB) magma(Davis et al., 2011) or a reprocessed subcontinental magma(Mckenzie and Oniins, 1995). Regional studies of the rock chemistry indicate a large-scale magmatic event.

CC BY 4.0 https://creativecommons.org/licenses/by/4.0/

Accepted manuscript (author version)

2. **Variations of Al^{4+} + Na versus Al^{6+} + 2Ti + Cr for estimating oxygen fugacity** (Schweitzer et al., 1979)

Oxygen fugacity exerts a marked influence on the liquidus temperature and the composition of both the melt and the crystallizing phases (France et al., 2010) and is a key factor controlling magmatic processes (Kilinc et al., 1983; Kress and Carmichael, 1991; Ottonello, 2001; Moretti, 2005; Botcharnikov, 2005). It also affects the crystallization sequence and the types of minerals that form. Using the diagram of Al^{4+} + Na versus Al^{6+} + 2Ti + Cr—which is in turn dependent on the trivalent iron content in the pyroxenes—allows for an estimation of oxygen fugacity.

This diagram is based on the aluminum balance between the tetrahedral (Al^{4+}) and octahedral (Cr^{3+} and others) positions. In clinopyroxenes, Fe^{3+} can substitute for other trivalent elements such as Al^{4+}, Ti, and Cr in the octahedral site; hence, the amount of Fe^{3+} in pyroxenes depends on the available Al^{4+} and, in other words, reflects the aluminum balance between the tetrahedral and octahedral sites. Samples that plot above the 0 = Fe^{3+} line crystallized under high oxygen fugacity, while those below indicate low oxygen fugacity. Cameron and Papike, (1981) also emphasized that the greater the distance of a sample from the Fe^{3+} line, the higher the oxygen fugacity in its formation environment. In the present diagram, the samples are mostley fall below the 0 = Fe^{3+} line (Fig. 5).

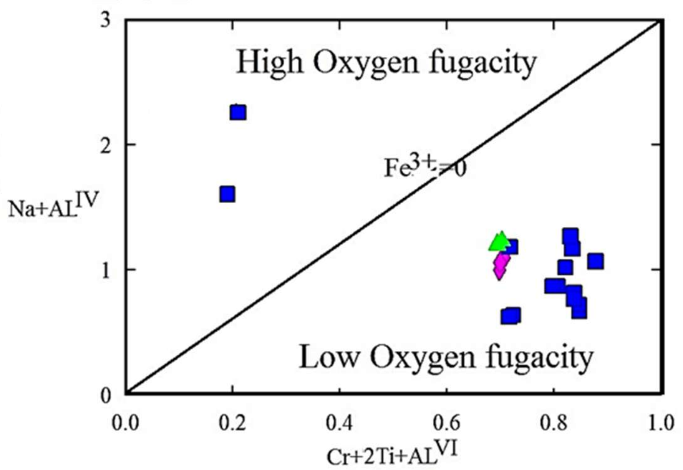

Figure 5. Diagram Al^{IV}+Na versus Al^{VI}+2Ti+Cr (Schweitzer et al., 1979)

CC BY 4.0 https://creativecommons.org/licenses/by/4.0/

Accepted manuscript (author version)

3. Geothermobarometry and Geobarometry

As shown in the ternary Ab–An–Or diagram (Fig. 6), the plagioclase of the studied samples formed at temperatures ranging from approximately 750 to 1100 °C and at pressures of about 1 kbar. Additionally, a clinopyroxene thermometer was applied to the regional rocks, yielding temperatures of approximately 900 to 1150 °C (Fig. 6).

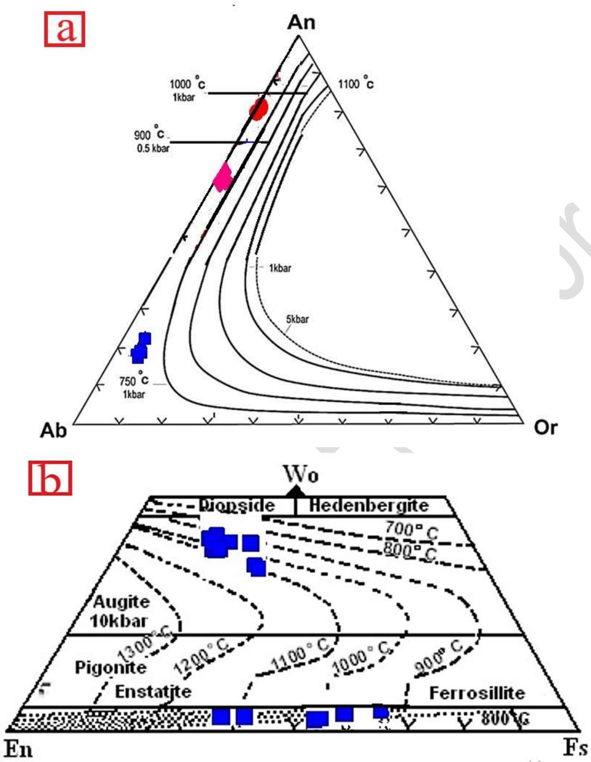

Figure 6. a- b-The Wo–En–Fs diagram for clinopyroxene used for temperature estimation (Lindsley, 1983).

For pressure estimates, (Wass, 1979) suggested that the ratios of Al^{VI}/Al^{IV}, $(Ti + Al^{IV})/Si$, and $TiO_2/(Mg + Mg + Fe)$ in pyroxenes can serve as geobarometers. In the Al^{VI}/Al^{IV} diagram, the samples fall within an intermediate pressure range (Fig. 5a). In clinopyroxenes, chromium is in equilibrium with Al^{VI}, and the ratio $Cr \times 100/(Cr + Al^{VI})$ in pyroxenes shows a direct relationship with pressure (Nimis and Taylor, 2000). In clinopyroxenes containing aluminum, high-pressure conditions are associated with the reaction:$NaAlSi_3O_8 \rightarrow NaAlSi_2O_6 + SiO_2$ while at lower pressures the reaction: $CaAl_2Si_2O_6 \rightarrow CaAl_2Si_2O_6 + SiO_2$ controls the system(Green and Ringwood, 1967). The first reaction occurs at greater depths (around 120 km, containing garnet–peridotite assemblages) and the second at depths of less than 40 km. For estimating the depth of

CC BY 4.0 https://creativecommons.org/licenses/by/4.0/

the magmatic reservoir, the aluminum distribution in clinopyroxenes is used. Researchers such as (Helz, 1983) have stressed that the distribution of aluminum between tetrahedral and octahedral sites in clinopyroxenes provides a good indicator for estimating the water content of the magma and the pressure conditions during the formation of the igneous rocks. With this model, a pressure of about 5 kbar is deduced for the crystallization of the pyroxenes, along with a magma water content of less than 10% (Fig. 7b).

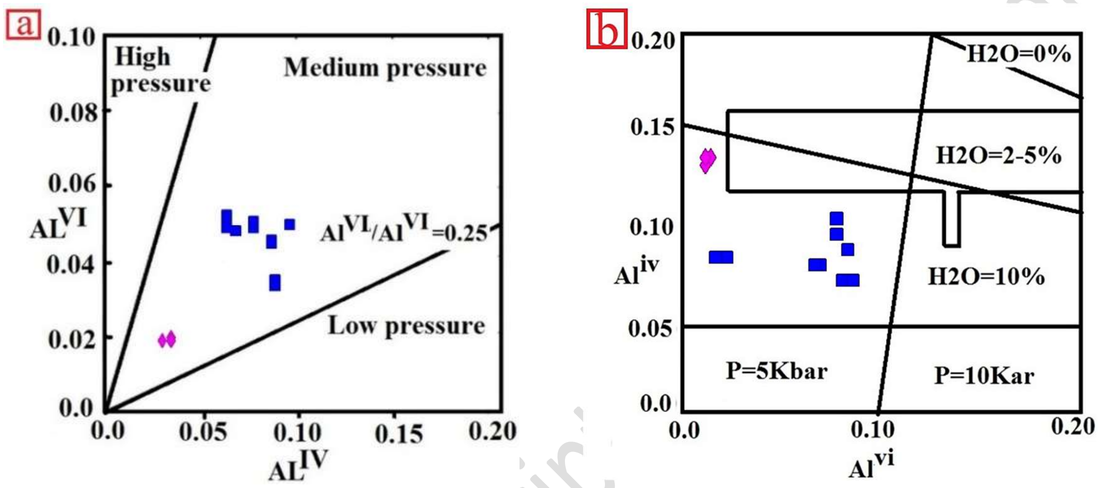

Figure 7. a-Barometric diagram of clinopyroxene using Al^{IV} versus Al^{VI} Aoki and Shiba, 1973). b- Barometric and hydrometric diagram for clinopyroxene(Helz, 1983).

The Ti/Al ratio in clinopyroxene compositions imposes constraints on their crystallization pressure conditions (for example Dobosi and Horváth, 1988; Wilkinson, 2001; Wlodyka, 2002; Ali and Ntaflos, 2011). The average Ti/Al ratio in the cores of clinopyroxenes from Pol-e Sefid is approximately 17, whereas in the rims it is about 22 (Fig. 5). The lower Ti/Al ratio in the cores indicates that they must have crystallized at relatively higher pressures compared to the rims. A table (not shown here) summarizes the temperature and pressure results calculated using the Excel file for clinopyroxene data (Putirka, 2008).

CC BY 4.0 https://creativecommons.org/licenses/by/4.0/

Accepted manuscript (author version)

Table 4. Temperature and pressure results calculated by Excel file for clinopyroxene mineral(Putirka, 2008).

	Putirka et al (2003)			Putirka (2008) RiMG MODELS		Barometers (and thermometer) based on Cpx compositions only Putirka (2008) RiMG			
				Eqn 34	Eqn 34	Eqn 32a	Eqn 32b	Eqn. 32c	Eqn. 32d
	T(K)	P(kbar)	T(C)	T(C)	T(C)	P(kbar)	P(kbar)	P(kbar)	T(C)
BR2	110.25	7.25	973.2	867.4	857.4	-	-	-	-
A45	1240.9	6.32	967.8	810.1	910.1	8.8	3.0	7.5	1129.4
2B	1255.4	6.20	983.2	919.3	919.13	6.3	4.2	8.5	1135.9
B3	0.0	5.5	978.2	895.6	998.6	-	-	8.9	-
A10	1052.6	7.1	950.4	930.13	962.9	8.7	8.7	6.10	-
A37	1023.6	7.1	945.4	942.11	952.9	8.5	8.7	6.17	-
A38	1013.6	7.1	948.4	952.13	932.9	8.3	8.7	6.25	-

4. Tectonic Environment:

In the Central Alborz, extensional tectonics began during the Mesozoic, with a rift-related volcanism initiated in the Upper Triassic simultaneously with the onset of coal-bearing sedimentation of the Shemshak Formation (Berberian & Berberian, 1981). This extensional phase, accompanied by regional normal faulting, led to widespread volcanism and plutonism in the area (Berberian & Berberian, 1981). The extensional processes, along with the related magmatism and plutonism in the Central Alborz, continued from the onset of the Triassic (marked by the initial deposition of the Shemshak Formation) until the end of the Triassic (concluding the deposition of the Shemshak formation(Fürsich et al., 2005; Berra et al., 2007; Zanchi et al., 2005; Zanchi et al., 2006; Samarbakhsh et al., 2023). In the first phase, with the onset of the Triassic, a shallow sea covered a large portion of the Iranian plate. During the Middle Triassic, the formation of the dolomitic carbonates of the Elika Formation in the Alborz, the Shotori Formation in Central Iran, and the evaporitic dolomites of the Khane Kat unit in the Zagros occurred. By the end of the Middle Triassic, due to the pre-Simmerian orogenic phase, the collision between the Sibmarine margin of the Alborz and the Lurian margin of the Turan resulted in the closure of the Paleotethys and the establishment of a continental environment. Concurrently, with the closure of the Paleotethys, the subduction of the Neotethys in the Zagros began, generating an extensional back-arc setting. This resulted in the activation of deep faults and the eruption of alkaline basaltic magmas in the Central

CC BY 4.0 https://creativecommons.org/licenses/by/4.0/

Alborz and Central Iran. In the second phase, due to the proximity of the Central Alborz and Central Iran to the equator and the prevailing hot climatic conditions—coupled with the availability of primary materials (basalts) and a suitable host rock (fractures and karsts in the carbonate units of the Elika and Shotori formations)—the best conditions for bauxitization via the weathering of basalts and various materials were established during the Upper Triassic. In these conditions, mobile elements in the basalts, such as alkali elements and silica, were leached out while the residual soils became enriched in immobile elements like aluminum, iron, and titanium. In the third phase, due to the uplift and erosion of the Alborz following the orogenic phase during the Upper Triassic to Liassic, the molasse sediments of the Shemshak Formation were deposited in intermontane basins. The synchronous sedimentation of this unit protected the bauxites from erosion. In the Pol-e Sefid area, the geochemical characteristics of the rocks indicate a within-plate magmatic (tectonomagmatic) affinity, forming in an extensional environment in the Late Triassic.

Based on the pressure measurements, the formation of magmatic reservoirs at the depth of the lower to middle crust is inferred as a likely environment for the growth and equilibrium of phenocrysts. Several factors influence the ascent of magma and the depth at which it is emplaced, including the structure, composition, age, and thermal and tectonic conditions of the crust (Chaussard and Amelung, 2014).

The composition of the crust affects the density contrast between the magma and the surrounding host rock, thereby influencing the magma's buoyancy and ascent rate. Additionally, the age and thickness of the crust are closely related to the depth of magma emplacement: shallower magmatic chambers (approximately 5 km depth) tend to occur more frequently in younger and thinner crusts.

Thermal conditions within the crust also play a critical role, as they influence the temperature differential between the ascending magma and the host rock, which in turn affects buoyancy forces. From a tectonic perspective, shallow magmatic chambers are more commonly associated with extensional and strike-slip regimes than with compressional settings. In extensional crusts, the reduced lithostatic pressure and presence of normal faulting facilitate magma ascent, increasing the likelihood of emplacement at shallower depths. Therefore, the pressure data obtained in this study may be more consistent with a relatively thin crust, possibly shaped by an extensional tectonic regime (Fig. 8).

CC BY 4.0 https://creativecommons.org/licenses/by/4.0/

Accepted manuscript (author version)

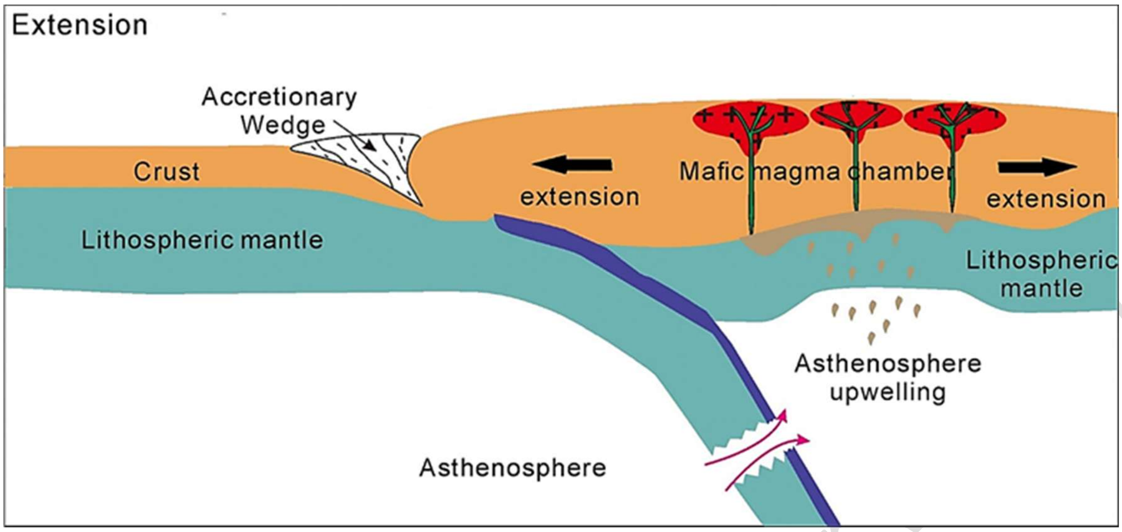

Figure 8. Schematic image of the formation of rocks in the area inspired by the design (Liu et al., 2021).

5. Discussion

Geochemical analyses of key minerals also suggest that these rocks were generated in an extensional tectonomagmatic environment. The chemical compositions and crystallization trends of the minerals are consistent with conditions of lithospheric thinning and crustal extension. These observations are in good agreement with field evidence and the presence of basaltic and trachybasaltic volcanic units in the studied area.

The findings of this study, indicating the formation of the Pol-e Sefid volcanic rocks in an extensional regime during the Late Triassic, are comparable with the present-day active tectonic framework of the Central Alborz. Seismotectonic investigations and active fault studies (e.g., Arian et al., 2012; Razaghian et al., 2018) demonstrate that part of the crustal stress field in this region still exhibits extensional characteristics. This consistency suggests that the tectonic processes responsible for the Late Triassic magmatism were part of a long-term geodynamic evolution, and that the identified extensional regime was not merely a short-lived event but is also linked to the current active tectonic trends. Therefore, integrating thermobarometric data with evidence from active tectonics provides a more comprehensive understanding of the geodynamic evolution of the Central Alborz.

CC BY 4.0 https://creativecommons.org/licenses/by/4.0/

6. Conclusions

The study area lies in the Central Alborz zone. The lithostratigraphic units here date from the Triassic to the Quaternary. Key formations include the Elika, Shemshak, and Lar formations, which are from the Triassic and Jurassic periods. Field and petrographic studies show that the volcanic rocks in the Pol Sefid region consist of basalt, olivine basalt, trachy basalt, and olivine dolerite. These rocks exhibit porphyritic, microlitic porphyritic, trachytic, intergranular, and intersertal textures. Main minerals include olivine, plagioclase (ranging from labradorite to anorthite), and pyroxene (augite). Secondary minerals are calcite, chlorite, and sericite. Clinopyroxene and plagioclase are the most significant minerals in these rocks. The chemical composition of pyroxenes suggests that the oxygen fugacity of the forming magmas varied, showing both low and high levels. Clinopyroxene composition indicates the alkaline nature of the parent melt. Thermobarometric results from clinopyroxene and plagioclase in the volcanic rocks of the Pol-e Sefid area show crystallization at temperatures around 900–1100 °C and pressures of 6–8.5 kbar. These P–T conditions align with a shallow extensional regime, where Late Triassic basaltic magmatism developed in the Central Alborz. Petrographic evidence further supports the basaltic nature of the magma and the extensional tectonic setting during its formation.

References

Ali S., Ntaflos T. (2011) Alkali basalts from Burgenland, Austria: petrological constraints on the origin of the westernmost magmatism in the Carpathian–Pannonian region. *Lithos* 121:176-188. DOI: https://doi.org/10.1016/j.lithos.2010.11.001

Aoki K., Shiba I. (1973) Pyroxenes from lherzolite inclusions of Itinome- Gata, Japan. *Lithos* 6(1): 41-51. DOI: https://doi.org/10.1016/0024-4937(73)90078-9

Arian M., Bagha N., Khavari R., Noroozpour H. (2012) Seismic Sources and Neo-Tectonics of Tehran Area (North Iran). *Indian Journal of Science and Technology* 5:2379-2383. DOI: https://dx.doi.org/10.17485/ijst/2012/v5i3.21

Arjmandzadeh R.,, Sharifi Teshnizi E., Ahmadi A.A., Mahdavi A., Tavsoli S., Dabiri R. (2021) The mineralogy, geochemistry and genesis of Aghol-Messi sedimentary copper-uranium deposit,

CC BY 4.0 https://creativecommons.org/licenses/by/4.0/

Tabas block, Central Iran, *Researches in Earth Sciences,* 11(4): 47-70. DOI: https://doi.org/10.52547/esrj.11.4.47

Assereto R. (1966a) The Jurassic Shemshak Fomation in central Alborz(Iran). *Rivista Italian Di paleontological e stratigrafa* 72: 1133-1182.

Berberian F., Berberian M. (1981) Tectono-plutonic episodes in Iran.In: Gupta HK, Delany FM (eds) Zagros, Hindukosh, Himalaya Geodynamic Evolution. American Geophysical Union,Washington DC: 5–32.

Berberian M., King G. C. P. (1981) owards a paleogeography and tectonic evolution of Iran. *Canadian Journal of Earth Sciences* 18(2):210-265.

Berra F., Zanchi A., Mattei M., Nawab A. (2007) Late Cretaceous transgression on a Cimmerian high (Neka Valley, Eastern Alborz, Iran): A geodynamic event recorded by glauconitic sands. *Sedimentary Geology* 199:189-204. DOI: https://doi.org/10.1016/j.sedgeo.2007.02.001

Botcharnikov R. E., Koepke J., Holtz F., McCammon C., Wilke M. (2005) The effect of water activity on the oxidation and the structural state of Fe in a Ferro-basaltic melt. *Geochimica et Cosmochimica Acta* 69:5071-5085. DOI: https://doi.org/10.1016/j.gca.2005.04.023

Cameron M., Papike J. (1981) Structural and chemical variations in Pyroxenes. *American Mineralogist* 66:1-50.

Chaussard E., Amelung F. (2014) Regional controls on magma ascent and storage in volcanic arcs. *Geochemistry, Geophysics, Geosystems* 15(4):1407-1418. DOI: https://doi.org/10.1002/2013GC005216

Dabiri R., Akbari-Mogaddam M., Ghaffari M. (2018) Geochemical evolution and petrogenesis of the eocene Kashmar granitoid rocks, NE Iran: implications for fractional crystallization and crustal contamination processes, *Iranian Journal of Earth Sciences* 10 (1): 68-77.

Davis G. H., Stephen J., Reynolds C., Kluth F. (2011) Structural Geology of Rocks and Regions, 3rd Edition. *Structural geology*. 864 P.

Deer W.A., Howie R.A., Zussman J. (1991) An introduction to the Rock-Forming Minerals, 17th Edition, Longman, London.

CC BY 4.0 https://creativecommons.org/licenses/by/4.0/

Accepted manuscript (author version)

Dobosi G., Horváth I. (1988) Highand low-pressure cognate clinopyroxenes from alkali lamprophyres of the Velence and Buda Mountains. *Neues Jahrbuch Fur Mineralogie-Abhandlungen* 158:2- 412.

Doroozi R., Vaccaro C., Masoudi F. (2017) Mesozoic alkaline plutonism: Evidence for extensional phase in Alpine-Himalayan orogenic belt in Central Alborz, north Iran, *Solid Earth Science* 91-108. DOI: https://doi.org/10.1016/j.sesci.2017.07.001.

Doroozi R., Vaccaro C., Masoudi F., Petrin R. (2018) Petrogenesis and mantle source characteristics of Triassic alkaline basaltic rocks of North Kamarbon, Northern Central Alborz, Iran. *Solid Earth Sciences* 3:115-129. DOI: https://doi.org/10.1016/j.sesci.2018.06.001

Fenner R.H. (1926) The Katmai magmatic province. *Journal Geology* 34: 673-772.

Finch R.H., Anderson C.A. (1930) The Quartz basalt eruptions of Cinder Cone, Lassen Volcanic National Park, California. *Cal Univ Pubs Geology Science* 19:245-273.

France L., Koepke J., IIdefonse B., Cichy S. B., Deschamps F. (2010) Hydrous partial melting in the sheeted dike complex at fast-spreading ridges: Experimental and natural observations. *Contributions to Mineralogy and Petrology* 160:683-704. DOI: https://doi.org/10.1007/s00410-010-0502-6

Fürsich F. T., Wilmsen M., Seyed-Emami K., Cecca F., Majidifard R. (2005) The upper Shemshak Formation (Toarcian-Aalenian) of the Eastern Alborz (Iran): biota and palaeoenvironments during a transgressive-regressive cycle. *Facies* 51:365-384. DOI: https://doi.org/10.1007/s10347-005-0051-z

Ghasemi H., Jamshidi K. (2012) Geochemistry, petrology and proposed tectonomagmatic model for generation of alkaline basic rocks in the base of the shemshak Formation, the Eastern Alborz Zone. *Iranian Journal of Crystallography and Mineralogy* 19(4):699-714 (in Persian).

Ghasemi H., Jamshidi K., (2013). Investigation of source region properties of alkaline basic rocks in the base of Shemshak Formation in the eastern Alborz zone. *Iranian Journal of Geology* 7: 17-29 (in Persian).

CC BY 4.0 https://creativecommons.org/licenses/by/4.0/

Ghasempour M.R., Ghazi J.M., Biabangard H., Dabiri R. (2014) Petrogenic significance of the Plio-Quaternary Nehbandan mafic lavas, Eastern Iran, *Iranian Journal of Earth Sciences,* 6(2): 133-141.

Goncalves P., Marquer D., Oliot E., Durand C. (2013) Thermodynamic modeling and thermobarometry of metasomatized rocks. In D. E. Harlov & H. Austrheim (Eds.), Metasomatism and the Chemical Transformation of Rock (Lecture Notes in Earth System Sciences, pp. 53‑??). Springer‑Verlag Berlin Heidelberg. DOI: https://doi.org/10.1007/978-3-642-28394-9_3

Green D.H., Ringwood A.E. (1967) An Experimental Investigation of the Gabbro to Eclogite Transformation and Its Petrological Applications. *Geochimica et Cosmochimica Acta* 31:767-833.

Helz R.T. (1983) Phase reactions of basalts in their melting rang at PH2O=5kb. Part II. Melt composition. *Journal of Petrology* 17:139-193.

Huot F., Hébert R., Varfalvy V., Beaudoin G., Wang C., Liu Z., Cotton J., Dostal J. (2002) The Beimarang mélange (southern Tibet) brings additional constraints in assessing the origin, metamorphic evolution andobduction processes of the Yarlung Zangbo ophiolite. *Journal of Asian Earth Sciences* 21(3):307-322.

Khosrow Tehrani Kh. (2007) Stratigraphy of Iran. Tehran University Press, 582 pp.

Kilinc A., Carmichael I. S. E., Rivers M. L., Sark R. O. (1983) The ferric-ferrous ration of natural silicate liquids equilibrated in air. *Contributions to Mineralogy and Petrology* 83:136-140.

Kress V.C., Carmichael I.S.E. (1991) The compressibility of silicate liquids containing Fe_2O_3 and the effect of composition, temperature, oxygen fugacity and pressure on their redox states. *Contributions to Mineralogy and Petrology* 108:82-92.

Larsen E. S., Irving J., Gonyer F. A. (1938) Petrologic results of a study of the minerals from the Tertiary volcanic rocks of the San Juan region, Colorado. *American Mineralogist* 23(7):417‑429. DOI: https://pubs.usgs.gov/pp/0524h/report.pdf?utm_source=chatgpt.com

CC BY 4.0 https://creativecommons.org/licenses/by/4.0/

Le Bas M.J. (1962) The role of aluminum in igneous. Clinopyroxenes with relation to their parentage. *American Journal of Science* 260:267-288.

Leterrier J., Maury R. C., Thonon P., Girard D., Marchal M. (1982) Clinopyroxene composition as a method of identification of the magmatic affinities of paleo-volcanic series. *Earth and Planetary Science Letters* 59: 139-154.

Lindsley D.H. (1983) Pyroxene Thermometry. *American Mineralogist* 68: 477-493.

Liu H. C., Shao J., Zhu G. Y., Li Y. L. (2021) Neoarchean basement, mantle enrichment and crustal extraction in central asia: Petrogenesis of 2.5 Ga amphibolite and metadiorite in NE China. *American Journal of Science* 321: 1350–1379. DOI: https://doi.org/10.2475/09.2021.03

Mckenzie D. P., ONiins R. K. (1995) The source regions of ocean island basalts. *Journal of Petrology* 36: 133-159.

Mollai H., Dabiri R., Torshizian H. A., Pe-Piper G., Wang W. E. (2021) Upper Neoproterozoic garnet-bearing granites in the Zeber-Kuh region from east central Iran micro plate: Implications for the magmatic evolution in the northern margin of Gondwanaland, *Geologica Carpathica* 72 (6): 461-81. DOI: https://doi.org/10.31577/GeolCarp.72.6.2

Moretti R. (2005) Polymerisation, basicity, oxidation state and their role in ionic modeling of silicate melts. *Annales Geophysicae* 56: 340–368. DOI: https://doi.org/10.4401/ag-3221

Morimoto N. (1988) Nomenclature of Pyroxenes. *Mineralogy and Petrology* 39: 55-76.

Nazari H. (2006) Analyse de la tectonique recente et active dans l Alborz Central et la region de Tehreran: Approche morphotectonique et paleoseismologique. theses PhD. Montpellier ll, Montpellier, France, p. 110. 10.1029.2004GL020058, 2004.

Nazari H., Omrani J., Shahidi A.R. (2004) Geological Map of Anzali, Scale 1:100000. Geological Survey of Iran.

Nazari H., Shahidi A., (2011) Tectonic of Iran «Alborz». Gological Survey and Mineral Exploration of Iran. *Research institute for Earth Science* 97 p.

Accepted manuscript (author version)

CC BY 4.0 https://creativecommons.org/licenses/by/4.0/

Accepted manuscript (author version)

Nimis P., Taylor W.R. (2000) Single Clinopyroxene Thermobarometery for Garnet Peridotites. Part I. Calibration and Testing of the Cr-in-Cpx Barometer and an Enstitite-in-Cpx Thermometer. *Contributions to Mineralogy and Petrology* 139:541-554. http://dx.doi.org/10.1007/s004100000156

Ottonello G., Moretti R., Marini L., Vetuschi Zuccolini M. (2001) Oxidation state of iron in silicate glasses and melts: A thermochemical model. *Chemical Geology* 174:157–179. DOI: https://doi.org/10.1016/S0009-2541(00)00314-4

Putirka K.D. (2008) Thermometera and barometers for volcanic systems. *Reviews in Mineralogy and Geochemistry* 69:61-120. DOI: https://doi.org/10.2138/rmg.2008.69.3

Razaghian G., Beitollahi A., Pourkermani M., Arian M. (2018) Determining seismotectonic provinces based on seismicity coefficients in Iran. *Journal of Geodynamics* 119:29-46. DOI: https://doi.org/10.1016/j.jog.2018.05.007

Rostami F., Delavari M., Dolati A. (2018) Mineral chemistry of the Permain basalta from North of Baladeh Central Alborz: Geotherbarometry and tectonomagmatic setting. *Scientific Quarterly Journal* of *GEOSCIENCES* 27:3-14. DOI: https://doi.org/10.22071/gsj.2018.58316

Saeedi A., Akbarpour M.R. (1992) Geological Map 1:100,000 of Kiasar, Publications of the Geological and Mineral Exploration Organization of the Country

Samadian M.R., Nabavi M.H., Alavi Naini M., Shahrabi M., Hamedi A.R., Vaezipour M.J., N.I.O.C., compiled by Aghanabati A., Hamedi A.R. (1994) Geological Map of Semnan, Geological Survey and Mineral Exploration of Iran, Scale 1:250,000.

Samarbakhsh S., Emami M.H., Mortazavi M., Abedini-Vosoughi M. (2023) Geochemistry and petrology of Upper Triassic basic volcanic rocks in the Central Alborz region, south of Pole Sefid. *Scientific Quarterly Journal* of *GEOSCIENCES* 33(127):161-178. DOI: https://doi.org/10.22071/gsj.2022.314965.1954

Sayari M. (2011) APG: An efficient software program for Amp-Pl thermobarometry based on graphical method. *Journal of Sciences* 22(4):345-349.

CC BY 4.0 https://creativecommons.org/licenses/by/4.0/

Accepted manuscript (author version)

Sayari M., Sharifi M. (2014) SCG: A computer application for single clinopyroxene geothermobarometry. *Italian Journal of Geosciences* 133(2):315-322. DOI: https://doi.org/10.3301/IJG.2014.01

Schweitzer E., Papike J., Bence A. (1979) Statistical analysis of clinopyroxenes from deep-sea basalts. *American Mineralogist* 64:501-513.

Shahabi Sh., Ghasemi H., Rezai Kahkhai M., Minggou Zh. (2021) Thermo-barometry of Permo-Triassic mafic igneous intrusion, Talu, Eastern Alborz Zone. *Scientific Quarterly Journal* of *GEOSCIENCES* 31(2): 173-188. DOI: https://doi.org/10.22071/gsj.2020.237027.1809

Talebian Borojenie H, Sheykhzakariaei S.J., Dabiri R., Yazdi A. (2025) Petrogenesis and tectonic implications of Neoproterozoic to Cenozoic A-type granitoids in NW Iran: geochemical and tectonic constraints, *Iranian Journal of Earth Sciences*, 17(4): 1-19. DOI: https://doi.org/10.57647/j.ijes.2025.16894

Vahabzadeh A. (2007) Geochemistry and genesis of fluorite deposits in Savadkouh region and presentation of their exploration model, PhD thesis, Shahid Beheshti University, Tehran, Iran, p.

Wass S. Y. (1979) Multiple origins of clinopyroxenes in alkali basaltic rocks. *Lithos* 12(2): 115-132.

Wilkinson J.J. (2001) Fluid Inclusions in Hydrothermal Ore Deposits. *Lithos* 55: 229-272. DOI: https://doi.org/10.1016/S0024-4937(00)00047-5

Wlodyka R. (2002) Clinopyroxene and amphibole zoning patterns in teschenite rocks from the outer western polish carpatians. Congress of Carpathian-Balkan Geological Association Bratislava. September 1st-4th.

Zanchi A., Berra F., Mattei M., Zanchetta S., Nawab, A., Sabouri, J. (2005) The early Mesozoic Cimmerian orogeny in the Alborz mountains, Iran. *Geophysical Research* 7: 1607-7962. 1607-7962.gra.EGU05-A-05696.

Zanchi A., Berra, F., Mattei M., Ghassemi M. R., Sabouri J. (2006) Inversion tectonics in Central Iran. *Journal of Structural Geology* 28: 2023-2037. DOI: https://doi.org/10.1016/j.jsg.2006.06.020

CC BY 4.0 https://creativecommons.org/licenses/by/4.0/